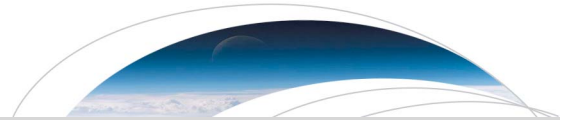


DOCKETED

Docket Number:	15-AFC-01
Project Title:	Puente Power Project
TN #:	215428-2
Document Title:	Testimony of Dr. Revell Exhibit Dynamic Models of an Earthquake and Tsunami offshore Ventura
Description:	AGU.Publications - Geophysical Research Letters
Filer:	PATRICIA LARKIN
Organization:	SHUTE, MIHALY & WEINBERGER LLP
Submitter Role:	Intervenor Representative
Submission Date:	1/18/2017 2:09:03 PM
Docketed Date:	1/18/2017



RESEARCH LETTER

10.1002/2015GL064507

Key Points:

- Dynamic earthquake and tsunami models offshore Ventura, California
- Our models show strong tsunami amplitudes northward and eastward toward Santa Barbara and Ventura

Supporting Information:

- Supporting Information S1
- Movie S1

Correspondence to:

K. J. Ryan,
kenny.ryan@email.ucr.edu

Citation:

Ryan, K. J., E. L. Geist, M. Barall, and D. D. Oglesby (2015), Dynamic models of an earthquake and tsunami offshore Ventura, California, *Geophys. Res. Lett.*, 42, doi:10.1002/2015GL064507.

Received 12 MAY 2015

Accepted 10 JUL 2015

Dynamic models of an earthquake and tsunami offshore Ventura, California

Kenny J. Ryan¹, Eric L. Geist², Michael Barall³, and David D. Oglesby¹

¹Earth Sciences, University of California, Riverside, California, USA, ²United States Geological Survey, Menlo Park, California, USA, ³Invisible Software, San Jose, California, USA

Abstract The Ventura basin in Southern California includes coastal dip-slip faults that can likely produce earthquakes of magnitude 7 or greater and significant local tsunamis. We construct a 3-D dynamic rupture model of an earthquake on the Pitas Point and Lower Red Mountain faults to model low-frequency ground motion and the resulting tsunami, with a goal of elucidating the seismic and tsunami hazard in this area. Our model results in an average stress drop of 6 MPa, an average fault slip of 7.4 m, and a moment magnitude of 7.7, consistent with regional paleoseismic data. Our corresponding tsunami model uses final seafloor displacement from the rupture model as initial conditions to compute local propagation and inundation, resulting in large peak tsunami amplitudes northward and eastward due to site and path effects. Modeled inundation in the Ventura area is significantly greater than that indicated by state of California's current reference inundation line.

1. Introduction

Earthquakes are among the chief sources of tsunamis—long ocean waves sustained by gravity that increase in amplitude as water depth decreases. Therefore, such waves are particularly hazardous along populated coastlines near offshore faults that produce vertical displacement of the seafloor and water column. Although the hazard from earthquake-generated tsunamis offshore Southern California has received relatively little attention, there have been reports of several significant local tsunamis in the past 200 years [Townley and Allen, 1939; Ulrich, 1942; Lander et al., 1993; Borrero et al., 2001]. Lander et al. [1993] explain that both locally generated tsunamis (e.g., tsunamis generated from the 1812 and 1854 Santa Barbara earthquakes and possible submarine landslides) as well as far-field generated tsunamis (e.g., the tsunami generated from the 1946 Aleutian earthquake) have impacted the California coast. In particular, the 1812 Santa Barbara earthquake (that likely occurred in the Santa Barbara Channel), estimated to have a local magnitude (M_L) of 7 [e.g., Hamilton et al., 1969], created a tsunami throughout the region that was reported as a “huge” sea wave [Townley and Allen, 1939], while the earthquake ground motion significantly damaged Mission San Buenaventura in Ventura [Townley and Allen, 1939].

Due to propagation speeds of ~ 700 km/h, tsunamis generated by distant sources allow for early coastal warning on the order of hours. However, tsunamis generated locally by faulting and landslides offshore California can impact the California coastline in a matter of minutes, making it imperative to understand the likelihood of such events. Ross et al. [2004] examined seismic and secondary hazards (e.g., tsunamis and liquefaction) along the coast of Ventura County, California, suggesting that the area is at risk of damaging tsunamis from both the far field (e.g., offshore Alaska) and the near field (e.g., Santa Barbara Channel). Wilson et al. [2014] conducted a California statewide survey to examine possible evidence from tsunami impacts along the coastline, including 20 coastal marshlands. Potential tsunami deposits were assessed at the Carpinteria Salt Marsh Reserve in Santa Barbara County. In particular, at this location they found sand layers consistent with tsunami deposition. However, observed microfossils in those same sand layers did not have a marine origin. Therefore, current evidence of prehistoric tsunamis impacting the Carpinteria Salt Marsh Reserve is somewhat ambiguous.

The ground motion from submarine earthquakes can generate tsunamis, and studies have shown that the ground motion distribution depends quite strongly on the geometric pattern of ruptured faults [e.g., Nason, 1973; McGarr, 1984; Cocco and Rovelli, 1989; Abrahamson and Somerville, 1996; Oglesby et al., 1998]. Therefore, fault geometry can have first-order effects on tsunami generation [Wendt et al., 2009]. The distribution of slip on a fault can have important effects on the generated tsunami as well [Geist, 1998;

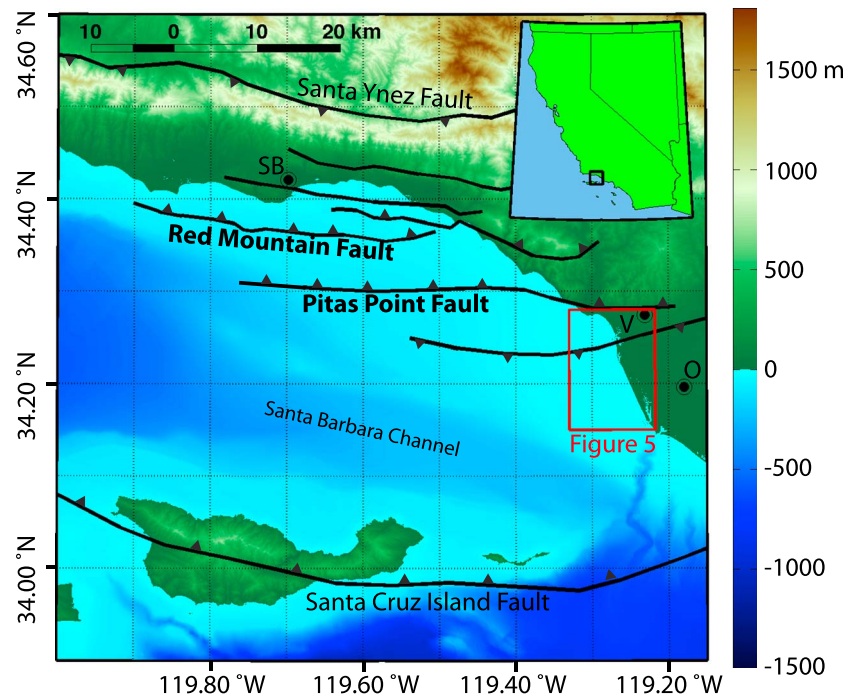


Figure 1. Topographic/bathymetric map of onshore/offshore Southern California, with height and depth in meters. The Red Mountain and Pitas Point faults are considered in this study. Triangles indicate direction of dip; faults without triangles are considered strike slip. Letters show approximate (central) city locations: SB = Santa Barbara, V = Ventura, O = Oxnard. The rectangle outlined in red contains the geographic region for Figure 5. Inset shows the map boundary in black.

Geist and Dmowska, 1999; Geist, 2002]. Unfortunately, the rupture path and slip pattern of an earthquake on a complex fault system are not easy to estimate a priori. Dynamic earthquake rupture models are a useful way of providing realistic earthquake scenarios on geometrically complex faults; such models are physics-based and do not assume a fault slip distribution or ground motion a priori; rather, slip distribution and ground motion are calculated results of the models based on estimates of fault stress, geometry, and material properties. The use of such methods in tsunami modeling is quite new; to date, only *Wendt et al. [2009]* has used dynamic rupture modeling to estimate tsunami generation from geometrically complex faults. Furthermore, there have been few tsunami modeling studies offshore Ventura, California (see Figure 1). *Borrero et al. [2001]* perform hydrodynamic analysis from a locally generated tsunami offshore Southern California on the Channel Islands Thrust system, a north dipping fault that is located approximately 50 km south of Santa Barbara. Assuming a homogeneous slip distribution on a planar fault, they find regional tsunamis with about 2 m of runup from a moment magnitude (M_w) 7.3 earthquake source and up to 15 m of local runup from submarine landslides that could be triggered from nearby earthquakes. However, they do not incorporate any geometrical complexity or spatially heterogeneous slip in their earthquake models, nor do they investigate potential tsunamis from other offshore reverse faults in the region, including the Red Mountain and Pitas Point faults, which are closer to some populated regions. The Pitas Point and Red Mountain faults are north dipping and generally trend east-west [e.g., *Fisher et al., 2009*]. *Hubbard et al. [2014]* used several available data sets, including industry seismic profiles as well as their own seismic profiles to improve the subsurface fault model for this fault system. The model presented by *Hubbard et al. [2014]* suggests a complex, segmented fault system that extends to seismogenic depth (~ 20 km). *Rockwell [2011]* used aerial photography to identify marine terraces in the Ventura region along the coast of southern California, suggesting discrete movements in the past with 5–10 m of uplift, with the last event occurring approximately 800 years ago. Therefore, a proper tsunami hazard analysis should incorporate modeled earthquakes that produce deformation consistent with such events.

2. Dynamic Rupture on the Pitas Point and Lower Red Mountain Faults

We use a 3-D finite element method [*Barall, 2009*] to model earthquake rupture on a connected, nonplanar Pitas Point and Lower Red Mountain fault geometry (see Figures 1 and 2) with spatially constant initial

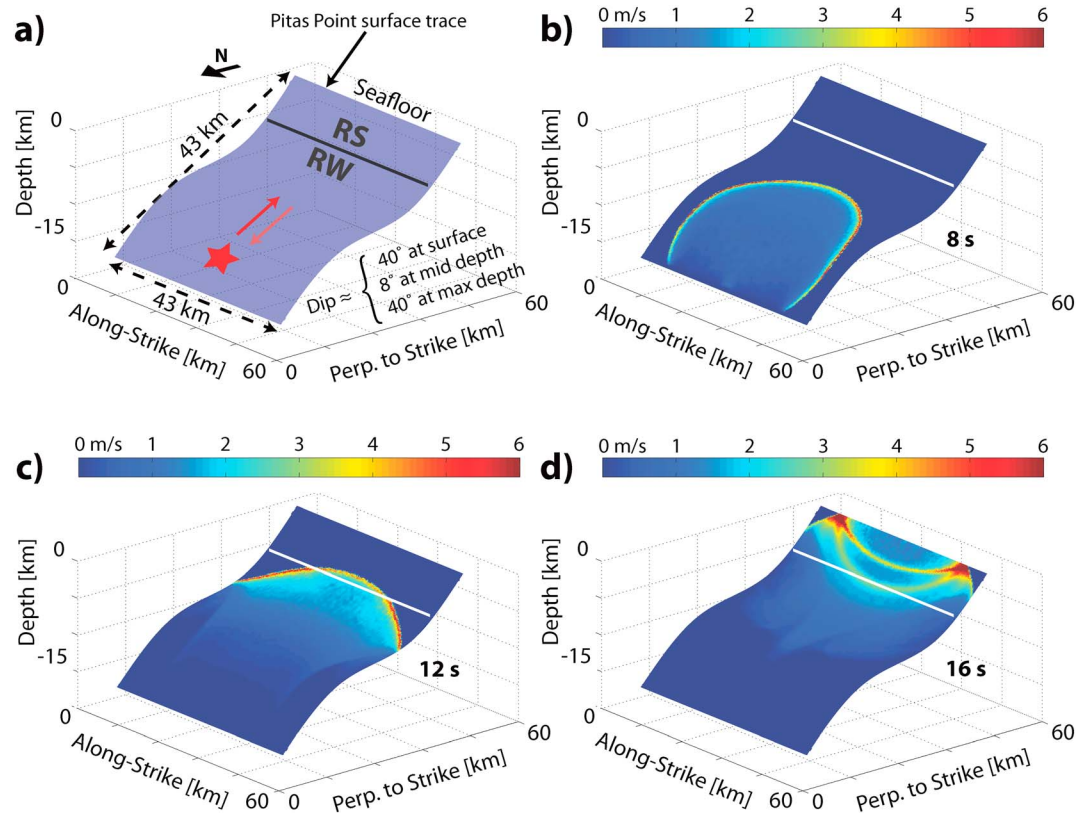


Figure 2. Fault geometry and slip rate snapshots. (a) The fault geometry of the connected Pitav Point and Lower Red Mountain faults with the rate-strengthening (RS)/rate-weakening (RW) boundary indicated by the solid black line (see Methods section), the nucleation zone indicated by the red star, and the approximate direction of fault slip indicated by the red arrows (i.e., reverse fault motion). Note that the Pitav Point fault intersects the seafloor and that fault dip is northward. (b–d) Dip-slip rate snapshots in m/s at 8 s, 12 s, and 16 s after earthquake nucleation, respectively. The solid white line indicates the RS/RW boundary.

traction and a homogeneous linear elastic Earth structure. The output consists of the rupture pattern on the fault as well as the full seismic wavefield and surface deformation. A key input is the fault system geometry. *Plesch et al.* [2007] developed a new 3-D community fault model for Southern California that consists of major fault systems defined by geologic and seismic evidence (e.g., surface traces and seismicity). *Hubbard et al.* [2014] further improved upon fault geometries both on and offshore Ventura County by utilizing additional data sets, including seismic reflection profiles and drill-hole data. Therefore, we use a fault system geometry consistent with *Hubbard et al.* [2014] to dynamically model earthquake rupture on the Pitav Point and Lower Red Mountain faults offshore Ventura. In particular, we utilize a fault geometry that connects the Pitav Point fault at depth to the deeper Lower Red Mountain fault via a more horizontal section of fault (see Figure 2). We employ a relatively curved fault geometry (e.g., the transition from the Lower Red Mountain fault to the Pitav Point fault is curved) that can result in a relatively smoother rupture transition along dip and slightly smoother ground deformation when compared to the kinked fault geometry in *Hubbard et al.* [2014] with analogous fault rupture. The resultant tsunami is not likely to be sensitive to these small spatial and temporal wavelength features.

The utilized material properties [e.g., *Christensen and Mooney, 1995*], prestress regime, and computational parameters (Table S1 in the supporting information) are quite generic and are not tuned to produce a worst case earthquake. FaultMod is validated in rupture benchmarks published by the Southern California Earthquake Center and the U.S. Geological Survey [*Barall, 2009; Harris et al., 2009*]. The code incorporates artificial viscous damping [*Dalguer and Day, 2007*] as well as algorithmic damping to help damp spurious oscillations and energy-absorbing boundary conditions along the mesh edges to avoid artificial seismic wave reflections from the model boundaries. Friction is a crucial part of earthquake processes. We use an

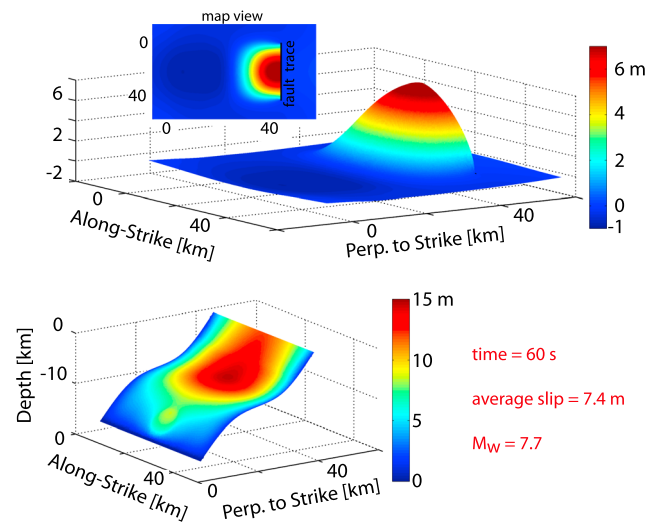


Figure 3. Vertical free surface deformation and total slip. (top) Vertical surface (i.e., seafloor) deformation resulting from slip on the fault system, with a maximum vertical displacement of over +7 m. The map view inset shows the same vertical deformation and indicates the fault trace by a solid black line. (bottom) Amplitude of slip on the fault system, with an average of 7.4 m. Note that the final deformation and slip are shown at 60 s after nucleation. The M_w for the earthquake is 7.7.

ment, approximately, when compared to the model that incorporates the rate-strengthening zone. Rupture nucleation (see red star in Figure 2a) is achieved by increasing the shear stress over an expanding front in time; following nucleation, rupture propagates along the rest of the fault spontaneously. The dynamic rupture code treats the seafloor as a traction-free surface and does not model the water movement (i.e., compressional waves through the water column are not modeled). The rupture model produces final seafloor displacement, which is then used as input for the tsunami modeling code.

The Cornell Multi-grid Coupled Tsunami (COMCOT) Model [Liu *et al.*, 1995; Wang and Liu, 2006] solves the discretized, nonlinear shallow-water wave equations, using an explicit leapfrog finite difference algorithm. The nonlinear convection term in the momentum equation is discretized using an upwind scheme. Attenuation from shear stress along the seafloor is included using Manning's formulation, where a constant Manning's coefficient of 0.013 is used. Runup and inundation over initially dry cells are also included through the implementation of moving boundary conditions. The merged bathymetric and topographic digital elevation models (DEMs) used for the tsunami model are from 1 and 3 arc sec resolution Southern California Coastal Relief Model version 2 from the National Geophysical Data Center. The reference elevation for both DEMs is mean sea level (MSL). A mean high water (MHW) vertical datum is used for the calculations by adjusting the DEMs according to the MHW-MSL difference listed at the Santa Barbara tide gauge station. The duration of the simulation is 160 min, sufficient for the maximum amplitude to be recorded in the model domain. Because the phase speed of tsunami waves is much slower than the velocity of the rupture front, particularly in the shallow ocean above the Pitas Point fault, the time-varying effects of tsunami generation are small [cf. Geist *et al.*, 2007]. Therefore, the instantaneous initial condition for tsunami generation is thought to be an adequate approximation.

The dynamic rupture model using the parameters listed in Table S1 results in a M_w 7.7 earthquake scenario on the Pitas Point and Lower Red Mountain faults. The fault geometry causes strong perturbations in slip rate that result from dynamic normal-stress perturbations as rupture travels updip [e.g., Oglesby *et al.*, 1998], with an average final slip of 7.4 m and an average static stress drop of approximately 6 MPa. Figure 2 shows the fault geometry and dip-slip rate snapshots at 8 s, 12 s, and 16 s. As rupture propagates updip, slip rate fluctuates owing to changes in fault geometry and consequent changes in dynamic normal stress. As rupture propagates through the first main bend, slip on the basal segment results in reduced normal stress (unclamping) on the connecting (nearly horizontal) section, which in turn results in increased slip rate on that connecting

empirically based rate- and state-dependent friction law [Dieterich, 1978, 1979; Ruina, 1983] that is controlled by physical parameters such as slip rate and time evolution of contact surfaces. Following the work of Lapusta *et al.* [2000] and Harris *et al.* [2009], we employ a modified version of the rate-state aging law that is computationally stable at very small slip rates [Ryan and Oglesby, 2014], with the bulk of the fault having rate-weakening (unstable) friction, and the top most 5 km of the fault having rate-strengthening (stable sliding) properties (see Figure 2). The depth extent of the modeled rate-strengthening zone is consistent with inferred stable sliding zones at subduction zones and crustal faults [e.g., Scholz, 1998]. We note that an analogous model without the rate-strengthening zone (i.e., completely rate weakening) has twice the average slip and twice the maximum vertical seafloor displacement,

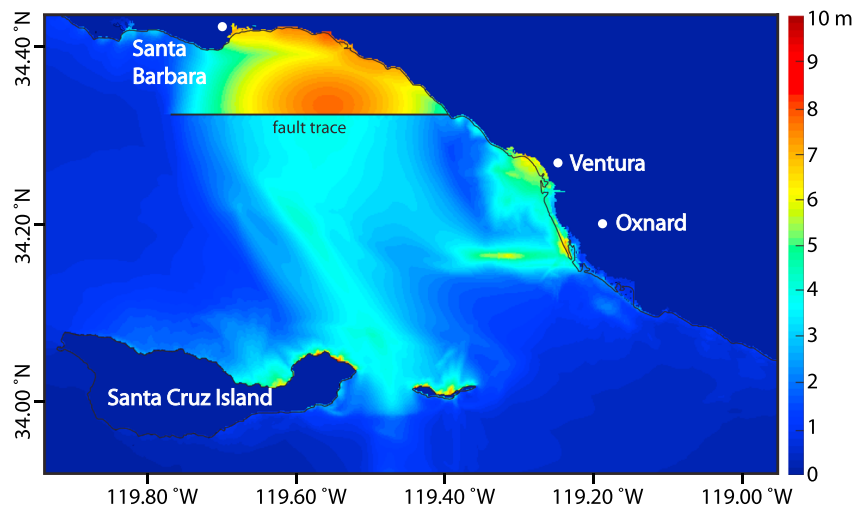


Figure 4. Map of regional peak tsunami amplitude in meters resulting from an earthquake on the Pitas Point and Lower Red Mountain fault system. The thin solid black line indicates the coastline, and the thick black line indicates the fault trace. Note that significant regional tsunami inundation occurs.

segment. As the rupture rounds the second fault bend the steeper updip section of fault is dynamically clamped, inhibiting fault slip; however, the rupture is strong enough to continue updip. At 12 s, the rupture is propagating into the rate-strengthening (stable) zone, resulting in reduced slip rate. Rupture extends to the free surface, with a breakout shown at 16 s. A breakout phase occurs when the rupture penetrates or “breaks out of” the free surface (i.e., seafloor) [e.g., *Oglesby et al.*, 1998]. At and around 16 s, there is a reduction in normal stress that corresponds to the breakout phase with an accompanying increase in slip rate.

Figure 3 shows vertical surface (i.e., seafloor) displacement and total slip resulting from the earthquake model. The largest vertical displacement, over 7 m, occurs on the hanging wall (north) side of the fault, consistent with observations of the Ventura fault—the onshore fault that is likely connected to the Pitas Point fault [e.g., *Rockwell*, 2011; *Hubbard et al.*, 2014]. The largest slip on the fault occurs updip from the nucleation zone (> -12 km depth), with somewhat reduced slip on the most updip section due to rate-strengthening friction. These results indicate that unclamping of normal stress induced by the updip-propagating rupture allows rupture to penetrate a rate-strengthening region near the surface [Ryan, 2012; *Kozdon and Dunham*, 2013]. Additionally, the curved fault geometry and constant traction result in an energetic rupture that produces significant slip within the surficial rate-strengthening zone, similar to that inferred in the 2011 Tohoku, Japan Earthquake [Yamazaki et al., 2011].

3. Local Tsunami Propagation and Inundation

The tsunami resulting from our modeled rupture on the Pitas Point and Lower Red Mountain faults (Figure 4) was modeled using COMCOT. The vertical displacement field calculated by the dynamic rupture models at 60 s provides the instantaneous initial condition for the tsunami model. Almost all of the fault slip occurs within the first 20 s of the model; the vertical displacement field at 60 s is the static configuration of the seafloor. The vertical seafloor displacement from the earthquake scenario produces a strong local tsunami wavetrain. Coastal areas with the largest local amplitude are northward (i.e., Santa Barbara) and eastward (i.e., Ventura and Oxnard) of the surface rupture. Large amplitudes northward result from the direct propagation of the northward-directed tsunami toward decreasing water depth as the tsunami approaches the coastline. The more unexpected large amplitudes to the east result from two main effects: strong eastward refraction of the southward directed tsunami wavetrain as the waves encounter deeper water to the south in the Santa Barbara Channel (Figure 1), and focusing of the waves guided by bathymetry (e.g., intersection of slower nearshore waves with faster deepwater waves in the channel). Figure 5 shows localized peak tsunami amplitude around Ventura and Oxnard, CA. Figure 1 outlines the area in Figure 5 in red. The solid black line indicates the coastline, and the solid red line is the statewide tsunami inundation border used by the California Emergency Management Agency [http://www.conservation.ca.gov/cgs/geologic_hazards/tsunami/inundation_maps/].

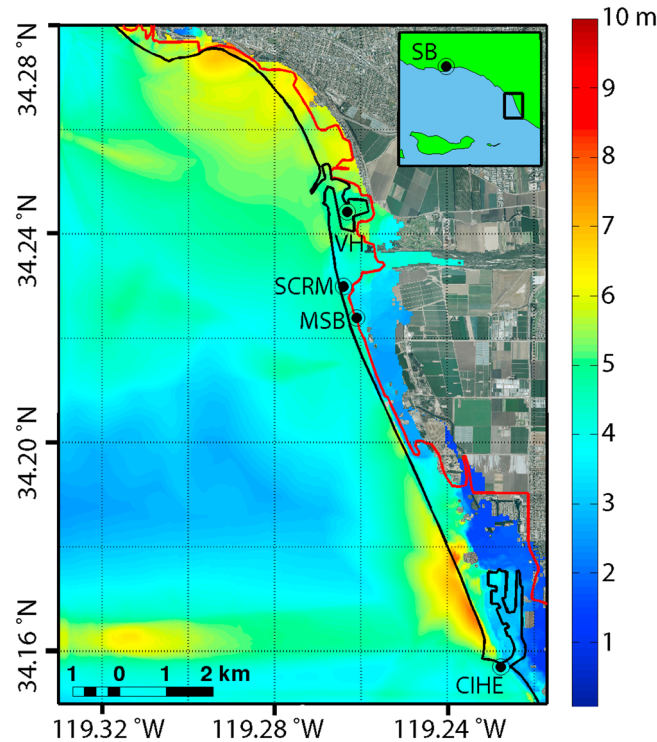


Figure 5. Map (red box shown in Figure 1) of localized peak tsunami amplitude, in meters (around Ventura, CA), resulting from slip on the Pitas Point and Lower Red Mountain fault system. The solid black line indicates the coastline. The solid red line is the statewide tsunami inundation map coordinated by the California Emergency Management Agency. Letters indicate example locations (approximate): SB = Santa Barbara, VH = Ventura Harbor, SCRM = Santa Clara River Mouth, MSB = McGrath State Beach, CIHE = Channel Islands Harbor Entrance. Inset shows the map boundary in black. Note that inundation from the model is significantly greater in many places than the statewide estimate.

Letters indicate key geographic locations, including Santa Barbara, Ventura Harbor, the Santa Clara River Mouth, McGrath State Beach, and the Channel Islands Harbor Entrance. Our modeled tsunami inundation exceeds the state estimate in multiple locations. For comparison, Figure S1 in the supporting information shows orthographic imagery of coastline indicated in Figure 5, with modeling results removed. Movie S1 in the supporting information shows how tsunami propagation from variations in the regional bathymetry leads to strong northward and eastward beaming effects. Note that inundation is not shown in the movie; Movie S1 is intended to show only propagation properties of the modeled tsunami. At less than 1 min, the surface break is apparent, with the tsunami splitting into two main waves propagating north and south. At approximately 9 min there are strong reflections of the northward wave off the northward shore and refraction (i.e., rotation counter clockwise) of the southward beaming tsunami due to water depth changes. Focusing occurs to the east (toward Ventura and Oxnard), shown at about 17 min, due to this refraction and reflection off local shorelines.

This study describes one potential earthquake and tsunami scenario along the Pitas Point and Lower Red Mountain

faults, but it is not intended to give an overall distribution of all possible earthquake and tsunami hazards in this region. The size of future earthquakes, their slip patterns, and thus their seafloor displacement are largely unknown a priori. It is therefore extremely helpful to combine dynamic earthquake models, which provide physically plausible earthquake scenarios in which the slip is a calculated result of the model, with tsunami models to study effects from tsunami generation and propagation; such models can help to fill in gaps in the historic and prehistoric record of earthquakes and tsunamis.

4. Implications for Tsunami Hazard Offshore Southern California

Generally, tsunamis can show complex wave effects, including reflection and refraction due to changes in topography/bathymetry along shorelines. Such wave properties have implications for tsunamis propagating along the southern California coastline. Results from the models in this study indicate that the coastal areas of Santa Barbara, Ventura, and Oxnard are particularly vulnerable to earthquake and tsunami hazard from rupture on the Pitas Point and Lower Red Mountain faults. Our modeled inundation exceeds, in most places, the state estimate of inundation in Ventura and Oxnard, owing to a combination of the seafloor displacement from our scenario earthquake, refraction, focusing, and flat topography that facilitates water flowing inland. Therefore, the tsunami hazard in Ventura and Oxnard may be higher than has been previously inferred. Additionally, we note that our earthquake model is not a worst case scenario, since we use (1) a stress parameterization that is not an outlier in terms of overall stress drop when compared to calculated stress drops in the southern California area [Hauksson, 2014] and (2) a somewhat conservative estimate for the spatial extent of the Pitas Point Fault (which may in fact connect to the Ventura fault on shore). However,

it is worth noting that the hypothetical earthquake scenario in this study would be among the top three or four largest magnitude earthquakes ever recorded in California, dating back to the mid eighteenth century [<http://earthquake.usgs.gov/earthquakes/eqarchives/>]. The probability of such an event in a given time frame is low compared to smaller earthquake events. Nonetheless, it is crucial to investigate the possible effects from such rare but plausible earthquake and tsunami scenarios so that a full hazard assessment can be made. While the details of an actual future event are likely to be more complex, our model likely captures many important aspects for the purposes of tsunami generation. Results from these modeling efforts can help reveal potential regions of high tsunami hazard. Additionally, further development of this methodology in tsunamigenic regions worldwide can contribute to hazard assessments.

We acknowledge some limitations in this study so that future studies can expand on the current results. The marine terraces along the coast could be the result of localized rupture effects since the uplift measurements are taken over a limited area [Hubbard *et al.*, 2014]. Additionally, multifault ruptures including, for example, the Ventura, Pitas Point, Red Mountain, and San Cayetano faults along the Ventura coast could produce the large amount of average slip needed to produce the terraces. The historical record for ruptures on the faults within this study is not well characterized; however, the available data suggest the possibility of large earthquakes with long recurrence intervals in this area, including multisegment ruptures producing earthquakes up to M_w 7.8 [Hubbard *et al.*, 2014]. Therefore, it will be important to model several different rupture scenarios on such fault systems, since the complete earthquake history of these faults is unknown. More comprehensive trenching onshore, sediment coring offshore, and sediment analysis onshore (i.e., sand grain analysis) to determine the occurrence of earthquakes and tsunami in this region are areas of active research [Wilson *et al.*, 2014]. Other regional reverse faults certainly have the capability of tsunamigenesis. The Santa Cruz Island and Anacapa-Dume faults, the largest known offshore fault zone near Ventura, CA, is 30 km to the south of the Pitas Point fault and is thought to be capable of generating large earthquakes with M_w greater than 7 [e.g., Pinter *et al.*, 1998; Ross *et al.*, 2004]. Incorporating the upper Red Mountain fault, which branches off near the intersection of the lower Red Mountain and Pitas Point faults, could strongly affect local tsunami properties in this area [Fisher *et al.*, 2005]. Finally, the current study assumes constant traction across the fault. However, we note that smaller magnitude stress regimes near the free surface would decrease the amount of energy available for seismic wave radiation and therefore would decrease, relative to the current model, fault slip near the free surface. Incorporating spatially varying initial stress distributions on the faults may provide valuable insight into a broader range of scenario ruptures. Earthquake size, rupture propagation, and slip distribution are directly dependent on nucleation location and stress regime [e.g., Oglesby *et al.*, 2008]. In addition, including elastic properties and plausible stress distributions from Global Positioning System models [e.g., Marshall *et al.*, 2013] may help provide robust, interdisciplinary earthquake and tsunami scenarios. We also note that submarine landslides can generate large tsunamis in and near the Santa Barbara Channel, and some landslides are documented in this region [Ross *et al.*, 2004; Fisher *et al.*, 2005]. In fact, modeling of the "Goleta Slide" indicates that a tsunami with local wave heights between 2 and 20 m could have been generated [Borrero *et al.*, 2001]. Our simple model is not complete enough to provide a true quantitative measure of tsunami hazard or the precise spatial extent of the inundation zone in the Ventura and Oxnard region; such a calculation would require the contribution of multiple faulting and landslide scenarios from a variety of near- and far-field sources. However, the current model gives an indication of what may be possible in this region and points toward future work to ameliorate the effects of tsunamis here and elsewhere around the globe.

Acknowledgments

The earthquake rupture code (FaultMod) used in this study is documented at <http://scecddata.usc.edu/cvws/download/codedesc/>. The tsunami code (COMCOT) used in this study is documented at <http://ceeserver.cce.cornell.edu/pll-group/comcot.htm>. We are especially grateful for conversations and help from Scott Marshall, Tom Parsons, Andreas Plesch, Tom Rockwell, James Dolan, and Surendra Sarkar. Additionally, we thank Judith Hubbard and Andrew Newman for their thoughtful comments and critiques that greatly improved this study. This work was supported by Southern California Earthquake Center award #14137. SCEC is funded by NSF Cooperative Agreement EAR-0529922 and USGS Cooperative Agreement 07HQAG0008.

The Editor thanks Judith Hubbard for her assistance in evaluating this paper.

References

- Abrahamson, N. A., and P. G. Somerville (1996), Effects of the hanging wall and footwall on ground motions recorded during the Northridge earthquake, *Bull. Seismol. Soc. Am.*, *86*, S93–S99.
- Barall, M. (2009), A grid-doubling finite-element technique for calculating dynamic three-dimensional spontaneous rupture on an earthquake fault, *Geophys. J. Int.*, *178*, 845–859.
- Borrero, J. C., J. F. Dolan, and C. E. Synolakis (2001), Tsunamis within the eastern Santa Barbara Channel, *Geophys. Res. Lett.*, *28*(4), 643–646, doi:10.1029/2000GL011980.
- Christensen, N. I., and W. D. Mooney (1995), Seismic velocity structure and composition of the continental crust: A global view, *J. Geophys. Res.*, *100*, 9761–9788, doi:10.1029/95JB00259.
- Cocco, M., and A. Rovelli (1989), Evidence for the variation of stress drop between normal and thrust faulting earthquakes in Italy, *J. Geophys. Res.*, *94*, 9399–9416, doi:10.1029/JB094iB07p09399.
- Dalguer, L. A., and S. M. Day (2007), Staggered-grid split-node method for spontaneous rupture simulation, *J. Geophys. Res.*, *112*, B02302, doi:10.1029/2006JB004467.

- Dieterich, J. H. (1978), Time-dependent friction and the mechanics of stick-slip, *Pure Appl. Geophys.*, *116*, 790–806.
- Dieterich, J. H. (1979), Modeling of rock friction 1. Experimental results and constitutive equations, *J. Geophys. Res.*, *84*, 2161–2168, doi:10.1029/JB084iB05p02161.
- Fisher, M. A., W. R. Normark, H. G. Greene, H. J. Lee, and S. W. Sliter (2005), Geology and tsunamigenic potential of submarine landslides in Santa Barbara Channel, Southern California, *Mar. Geol.*, *224*(1–4), 1–22.
- Fisher, M. A., C. C. Sorlien, and R. W. Sliter (2009), Potential earthquake faults offshore southern California, from the eastern Santa Barbara Channel south to Dana Point, *Geol. Soc. Am., Spec. Pap.*, *454*, 271–290.
- Geist, E. L. (1998), Local tsunamis and earthquake source parameters. Tsunamigenic earthquakes and their consequences, *Adv. Geophys.*, *39*, 117–209.
- Geist, E. L. (2002), Complex earthquake rupture and local tsunamis, *J. Geophys. Res.*, *107*(B5), 2086, doi:10.1029/2000JB000139.
- Geist, E. L., and R. Dmowska (1999), Local tsunamis and distributed slip at the source, *Pure Appl. Geophys.*, *154*, 485–512.
- Geist, E. L., V. V. Titov, D. Arcas, F. F. Pollitz, and S. L. Bilek (2007), Implications of the 26 December 2004 Sumatra–Andaman earthquake on tsunami forecast and assessment models for great subduction-zone earthquakes, *Bull. Seismol. Soc. Am.*, *97*(1A), S249–S270.
- Hamilton, R. M., et al. (1969), Seismicity and associated effects, Santa Barbara region, in geology, petroleum development, and seismicity of the Santa Barbara channel region, California, *U.S. Geol. Surv. Prof. Pap.*, *679-D*, 47–68.
- Harris, R. A., et al. (2009), The SCEC/USGS dynamic earthquake rupture code verification exercise, *Seismol. Res. Lett.*, *80*, 119–126.
- Hauksson, E. (2014), Average stress drops of Southern California earthquakes in the context of crustal geophysics: Implications for fault zone healing, *Pure Appl. Geophys.*, *1–12*, doi:10.1007/s00024-014-0934-4.
- Hubbard, J., et al. (2014), Structure and seismic hazard of the Ventura Avenue Anticline and Ventura Fault, California: Prospect for large, multisegment ruptures in the Western Transverse Ranges, *Bull. Seismol. Soc. Am.*, *104*, 1070–1087.
- Kozdon, J. E., and E. M. Dunham (2013), Rupture to the trench: Dynamic rupture simulations of the 11 March 2011 Tohoku earthquake, *Bull. Seismol. Soc. Am.*, *103*, 1275–1289.
- Lander, J. F., P. A. Lockridge, and M. J. Kozuch (1993), *Tsunamis Affecting the West Coast of the United States 1806–1992*, NGDC Key to Geophysical Records Documentation KGRD-29, pp. 242, U.S. Dep. of Commer., NOAA, Natl. Geophys. Data Cent., Boulder, Colo.
- Lapusta, N., J. R. Rice, Y. Ben-Zion, and G. Zheng (2000), Elastodynamic analysis for slow tectonic loading with spontaneous rupture episodes on faults with rate- and state-dependent friction, *J. Geophys. Res.*, *105*, 23,765–23,789, doi:10.1029/2000JB900250.
- Liu, P. L. F., Y. S. Cho, S. B. Yoon, and S. N. Seo (1995), Numerical simulations of the 1960 Chilean tsunami propagation and inundation at Hilo, Hawaii, in *Tsunami: Progress in Prediction, Disaster Prevention and Warning*, edited by Y. Tsuchiya and N. Shuto, pp. 99–115, Kluwer Acad., Netherlands.
- Marshall, S. T., G. J. Funning, and S. E. Owen (2013), Fault slip rates and interseismic deformation in the western Transverse Ranges, California, *J. Geophys. Res. Solid Earth*, *118*, 4511–4534, doi:10.1002/jgrb.50312.
- McGarr, A. (1984), Scaling of ground motion parameters, state of stress, and focal depth, *J. Geophys. Res.*, *89*, 6969–6979, doi:10.1029/JB089iB08p06969.
- Nason, R. (1973), Increased seismic shaking above a thrust fault, in *San Fernando, California, Earthquake of February 9, 1971*, pp. 123–126, U.S. Dep. of Commerce, Washington, D. C.
- Oglesby, D. D., R. J. Archuleta, and S. B. Nielsen (1998), Earthquakes on dipping faults: The effects of broken symmetry, *Science*, *280*, 1055–1059.
- Oglesby, D. D., P. M. Mai, K. Atakan, and S. Pucci (2008), Dynamic models of earthquakes on the North Anatolian fault zone under the Sea of Marmara: Effect of hypocenter location, *Geophys. Res. Lett.*, *35*, L18302, doi:10.1029/2008GL035037.
- Pinter, N., S. B. Lueddecke, E. A. Keller, and K. R. Simmons (1998), Late quaternary slip on the Santa Cruz Island fault, California, *Geol. Soc. Am. Bull.*, *110*(6), 711–722.
- Plesch, A., et al. (2007), Community fault model (CFM) for Southern California, *Bull. Seismol. Soc. Am.*, *97*(6), 1793–1802, doi:10.1785/0120050211.
- Rockwell, T. K. (2011), Large co-seismic uplift of coastal terraces across the Ventura Avenue anticline: Implications for the size of earthquakes and the potential for tsunami generation, Plenary talk presented at the Southern California Earthquake Center Annual Meeting, Palm Springs, Calif.
- Ross, S. L., et al. (2004), Comments on potential geologic and seismic hazards affecting Coastal Ventura County, California, *U.S. Geol. Surv. Open File Rep.*, *2004–1286*.
- Ruina, A. (1983), Slip instability and state variable friction laws, *J. Geophys. Res.*, *88*, 10,359–10,370, doi:10.1029/JB088iB12p10359.
- Ryan, K. J. (2012), Dynamic models of earthquake rupture on fault stepovers and dip-slip faults using various friction formulations, MS thesis, Dep. of Earth Sciences, Univ. of California, Riverside.
- Ryan, K. J., and D. D. Oglesby (2014), Dynamically modeling fault step overs using various friction laws, *J. Geophys. Res. Solid Earth*, *119*, 5814–5829, doi:10.1002/2014JB011151.
- Scholz, C. H. (1998), Earthquakes and friction laws, *Nature*, *391*, 37–42.
- Townley, S. D., and M. W. Allen (1939), Descriptive catalog of earthquakes of the Pacific coast of the United States 1769 to 1928, *Bull. Seismol. Soc. Am.*, *29*(1), 1–297.
- Ulrich, F. P. (1942), Progress report of the seismological work, United States Coast and Geodetic Survey in the Western United States During 1941, 1942.
- Wang, X., and P. L. F. Liu (2006), An analysis of 2004 Sumatra earthquake fault plane mechanisms and Indian Ocean tsunami, *J. Hydraul. Res.*, *44*(2), 147–154.
- Wendt, J., D. D. Oglesby, and E. L. Geist (2009), Tsunamis and splay fault dynamics, *Geophys. Res. Lett.*, *36*, L15303, doi:10.1029/2009GL038295.
- Wilson, R., et al. (2014), The search for geologic evidence of distant-source tsunamis using new field data in California, in *The SAFRR (Science Application for Risk Reduction) Tsunami Scenario, U.S. Geol. Surv. Open File Rep.*, *2013-1170-C*, edited by S. L. Ross and L. M. Jones, Chap. C, pp. 122, doi:10.3133/ofr20131170c.
- Yamazaki, Y., T. Lay, K. F. Cheung, H. Yue, and H. Kanamori (2011), Modeling near-field tsunami observations to improve finite-fault slip models for the 11 March 2011 Tohoku earthquake, *Geophys. Res. Lett.*, *38*, L00G15, doi:10.1029/2011GL049130.